Structural and electrical characterization of glasses in the Li_2O–CaO–B_2O_3 system

Pimentel N.B.[a], Mastelaro V.R.[b], M'Peko J.-C.[b], Martin S.W.[c], Rojas S.S.[a,c,*], De Souza J.E.[a,c]

[a] *Laboratório de Materiais Cerâmicos Avançados - LMCA, Faculdade de Ciências Exatas e Tecnologia, Universidade Federal da Grande Dourados - FACET-UFGD, CP 364, 79804-970, Dourados, MS, Brazil*

[b] *Grupo de Nanomateriais e Cerâmicas Avançadas - NaCA, Instituto de Física de São Carlos, Universidade de São Paulo - IFSC-USP, CP 369, 13560-970, São Carlos, SP, Brazil*

[c] *Glass and Optical Materials Group - GOM, Department of Material Science and Engineering, Iowa State University of Science and Technology - MSE-ISU, 2220E Hoover Hall, 50011-2300, Ames, IA, USA*

ABSTRACT

Glasses in the ternary $xLi_2O + (33-x)CaO + 67B_2O_3$ tetraborate system, with x = 0, 5, 10, 15, 20, 25, 30 and 33 mol%, were prepared by melting and casting. The glass structure, and thermal, and electrical response of highly transparent and homogeneous glasses were evaluated by X-Ray Diffraction (XRD), Differential Thermal Analysis (DTA), Fourier Transform Infrared Spectroscopy (FTIR) and Impedance Spectroscopy (IS). The glass transition temperature (T_g) decreases as CaO is substituted by Li_2O (increasing x), while the thermal stability against crystallization to the supercooled liquid in the region $T_g < T < T_l$, where T_l is the liquidus temperature, increases up to x = 20, according to $\Delta T \equiv (T_{oc} - T_g)$, where T_{oc} is the onset temperature of the first exotherm crystallization, and also considering the Hubrÿ's (K_H), and Weinberg's (K_W) thermal parameters. The short range order (SRO) structural change in this glass series is governed by the isomerization reaction $BØ_2O^- \Leftrightarrow BØ_4^-$, also designated as $B^2 \Leftrightarrow B^4$, where the superscript defines the number of bridging oxygens (BOs) on the SRO structural units. Li_2O substituting CaO in this tetraborate glass compositional series favors the formation of tetrahedral boron, B^4 SRO units, isomerization reaction for compositions up to 10 mol%. For glasses at higher lithium oxide contents, the reaction in the opposite direction is favored towards the formation of the metaborate B^2 SRO units. A dramatic increase in the ionic conductivity at 300 °C of more than 10 orders of magnitude was observed across this same compositional series. This dramatic increase is related to the higher mobility of the Li^+ ions, which has a smaller ionic radius, 0.59 Å (four-fold coordination) and a single ionic charge compared the significantly larger, 1.00 Å (six-fold coordination) and divalently charged Ca^{2+} ions in the glassy structure arrangement.

1. Introduction

Boron oxide, B_2O_3, is a typical glass forming compound that easily forms a glass with good thermal stability at a relatively low melting temperature. Borate glasses are known to possess both significant SRO and complex intermediate range order (IRO) structural units in the glassy network as a modifier compound, such as monovalent alkali oxide or a divalent alkaline earth oxide is added to B_2O_3 [1–3]. Further, these well studied alkali and alkaline earth doped borate (AAEB) glasses have also been shown to favor the acceptance of relatively large concentrations of rare-earth and transition metals dopants [4–6]. For these reasons, AAEB glasses have been widely studied in order to elucidate the complex SRO and IRO structures that are formed into the glass network due to changes in boron coordination number [7–9].

The primary SRO structural change in AAEB glasses is the widely studied formation of singly charged B^4 SRO units from neutral B^3 SRO units in the compositional range of $0 < x < 0.4$, where x is the mole fraction of the alkali or alkaline earth oxide in a binary AAEB glass. It is well known that the fraction of B4 units reach a maximum concentration of about 50% at about the tetraborate composition (~33 mol% of modifier) on nearly all AAEB glass systems [9–11]. This maximum of about 50% has been termed the so-called boron avoidance principle where reaching higher fractions of B4 units would require the direct bonding of B^4 SRO to each other through a BO and this appears to not

be favored due to both steric hindrance and the charge repulsion of the adjacent negatively charged B^4 SRO units. Therefore, beyond this maximum, the added alkali or alkali oxide causes the formation of progressively increasing numbers of terminally charged non-bridging oxygens (NBOs) in the form of B^2, B^1 and B^0 SRO units. For these reasons, glass formation in AAEB glasses falls off quickly beyond the B^4 maximum due to the rapid depolymerization of the glass network structure through the formation of the increasing number of NBOs. Nevertheless, in some cases, the lithium and sodium systems most notably, glasses can be formed even at the fully depolymerized B^0 composition, 75 mol% M_2O due to the presumably rapidly decreasing liquid temperatures of the melts [12, 13].

The complex structure associated with the presence of BOs and NBOs has a strong influence on the physical properties of AAEB glasses. For these reasons, AAEB systems have attracted significant attention of several researchers due to their interesting results concerning glass formation, structure, and properties [7–14].

Tetraborate compounds at the specific compositions of CaB_4O_7 and $Li_2B_4O_7$ are attractive materials because of their low hygroscopicity, low melting temperature when compared to silicates, high thermal stability, considerable transparency in the UV spectral region and promising application as thermoluminescent dosimeters [7, 8, 14].

Lithium borate glasses can be prepared in the $yLi_2O + (100-y)B_2O_3$ system, over the wide range of $0 \leq y \leq 75$ mol%, while calcium borate glasses can be obtained in the $yCaO + (100-y)B_2O_3$ binary system in the range of $33 \leq y < 50$ mol% [9, 13, 15]. In the last case, the lowest content for glass formation is set by the onset of a liquid-liquid phase separation, while crystallization processes brought on by the formation of large fractions of network degrading NBOs determine the upper limit [9, 13]. Rojas et al. have previously shown that the addition of 10 mol% of Li_2O to the CaB_4O_7 glass composition prevents the liquid-liquid phase separation in the lower modified compositions and allows the preparation of AAEB glasses at lower temperatures because of a decreasing in the T_g and T_l temperatures. It appears that there are only small changes in the glass structure due to this substitution [7].

It is also important to mention the limited number of papers, published in the literature, dealing with the ionic conductivity on alkali-earth oxide glasses [16]. For these reasons, the present study is directed towards a deeper compositional, structure, and property investigation of these mixed cation AAEB glasses starting from the CaB_4O_7 composition, with the gradual substitution of CaO by Li_2O. Glasses were prepared across the full calcium tetraborate CaB_4O_7 to lithium tetraborate $Li_2B_4O_7$ compositional series, in the $xLi_2O + (33-x)CaO + 67B_2O_3$ system with x = 0, 5, 10, 15, 20, 25, 30, 33 mol%. In the text, the compositions will be referred to as CaBO (x = 0), CaLiBO (x = 5 to 30) and LiBO (x = 33). The influence of changing CaO by Li_2O on thermal, structural and electrical properties of the glasses was investigated by X-ray Diffraction (XRD), Differential Thermal Analysis (DTA), Fourier Transform Infrared Spectroscopy (FTIR) and Impedance Spectroscopy (IS).

2. Materials and methods

To reduce moisture content in the glasses, precursor glass samples of B_2O_3 (Alfa Aesar, 99.98%) were previously prepared at 1300 °C for 3 h and maintained in desiccator to be used as raw material. The precursors $CaCO_3$ (CRQ-PA, 99%), Li_2CO_3 (Sigma-Aldrich-PA, 99%) and the previously prepared B_2O_3 glasses were precisely weighed (BEL M214Ai, ± 0.0001 g) in the required molar fraction as shown in Table 1. Batches of 20 g of each composition were prepared by melting and casting method in Pt/Au crucibles, in open air atmosphere, using resistive furnaces (EDG F1700 with elevator and EDG 30003P). The materials were heated to and held at 800 °C for 20 min to eliminate gases. The CaB_4O_7 composition was melted at 1450 °C and rapidly quenched to room temperature to avoid the liquid-liquid phase separation. The other samples were melted at temperatures between

1000 °C to 1100 °C, depending on the composition. Several homogenizations were done by swirling the liquid, in order to obtain homogeneous and bubble-free liquids and glasses. After 40 min at the melting temperature, the liquids were poured onto a pre-heated circular brass mold based on a stainless-steel plate. All the samples were annealed at temperatures between 400 °C and 550 °C, depending on the composition, for a period of 10 h and then slow cooled to room temperature.

The amorphous nature of the samples was confirmed by XRD using a Rigaku - Ultima IV 40 kV and 40 mA diffractometer with $CuK_{\alpha 1}$ radiation. Characteristic temperatures such as glass transition (T_g), onset of crystallization (T_{oc}), crystallization peak (T_{pc}) and liquidus temperature (T_l) were determined by Differential Thermal Analysis (DTA) technique using a Netzsch STA 409C thermal analyzer and Al_2O_3 as the reference. Samples in powder form, with particle sizes selected among 150 μm and 250 μm, were measured and placed into Al_2O_3 crucibles with synthetic air as atmosphere (20% O_2 and 80% N_2) at the heating rate of 10 °C/min.

Infrared absorption measurements were done by Attenuated Total Reflectance (ATR) spectroscopy in a Bruker Vertex 70 FT-IR spectrometer by using glasses in parallelepiped shapes with 2 mm in thickness. All the spectra were collected in the 600 to 4000 cm^{-1} spectral range with 2 cm^{-1} of resolution, at room temperature. The data were processed using the OPUS software, by applying *Rubberband Baseline Correction* tool to all spectra, and after that, applying the *Vector* normalization method.

The IS measurements were performed in the frequency range of 0.1 Hz to 1 MHz (10 points/decade), using a Solartron analyzer model SI 1260, coupled to the Dielectric Interface 1296A, both controlled by commercial SMART software. The analysis of the IS data was done using ZView software. The electric characterization was performed with vitreous samples cut in the shape of a parallelepiped, with thicknesses of approximately 0.5 mm, coated with Platinum (Pt) paint and previously treated at a temperature of 400 °C by 1 h to eliminate the organic solvents.

3. Results and discussion

3.1. Glass formation

AAEB glasses containing calcium and lithium oxides were prepared by the conventional melting and casting method. All the obtained samples were colorless and bubble-free glasses. The non-crystalline nature of all samples was confirmed by XRD spectra as presented in Fig. 1.
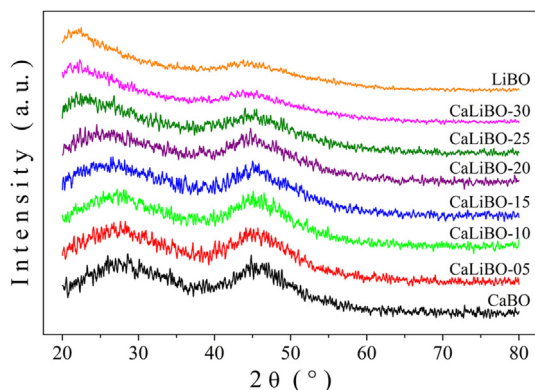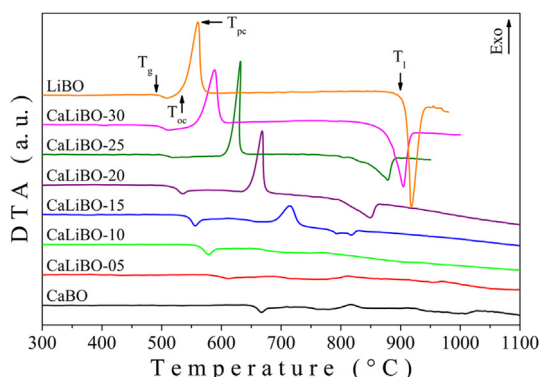
3.2. Thermal analysis

Thermal analysis measurements resulted in typical glass curves as seen in Fig. 2. The characteristic temperatures considered were the glass transition (T_g), onset of crystallization (T_{oc}), peak of crystallization (T_{pc}) and liquidus (T_l). Some thermal stability parameters, such as, $\Delta T \equiv T_{oc} - T_g$, $K_H \equiv (T_{oc} - T_g)/(T_l - T_{oc})$, the Hubrÿ's parameter, and $K_W \equiv (T_{oc} - T_g)/T_l$, the Weinberg's parameter, were also obtained and summarized in Table 1. These thermal stability parameters were applied because they have shown good agreement with the glass stability for different glass compositions according to the literature [15–18]. As these thermal parameters become larger, the higher will be the glass stability against crystallization on heating, as well as the glass forming ability [7, 15–18].

Glass transition behavior and thermal stability parameters (ΔT, K_H and K_W) as a function of Li_2O content is shown in Fig. 3. For a better comparison among the behavior of thermal parameters, the K_W values were multiplied by the factor 10 in Fig. 3. According to the gradual substitution of CaO by Li_2O in the AAEB glass system, a decrease in the T_g is seen, which varies from 655 °C (CaBO sample) to 492 °C (LiBO

Table 1
Nominal composition and characteristic temperatures (T_g, T_{oc}, T_{pc}, T_l) and thermal stability parameters (ΔT, K_H, K_W) obtained from DTA curves.

Sample	Nominal composition (mol%)	Thermal parameter						
		T_g (± 2 °C)	T_{oc} (± 2 °C)	T_{pc} (± 2 °C)	T_l (± 2 °C)	ΔT (± 4 °C)	K_H	K_W
CaBO	$67B_2O_3 + 33CaO$	655	791	817	924	136	1.02 ± 0.06	0.113 ± 0.004
CaLiBO-05	$67B_2O_3 + 28CaO + 5Li_2O$	586	773	811	917	187	1.29 ± 0.06	0.157 ± 0.004
CaLiBO-10	$67B_2O_3 + 23CaO + 10Li_2O$	562	750	768	890	188	1.34 ± 0.07	0.161 ± 0.004
CaLiBO-15	$67B_2O_3 + 18CaO + 15Li_2O$	544	691	714	784	147	1.6 ± 0.1	0.139 ± 0.004
CaLiBO-20	$67B_2O_3 + 13CaO + 20Li_2O$	518	650	668	797	132	0.90 ± 0.05	0.123 ± 0.004
CaLiBO-25	$67B_2O_3 + 8CaO + 25Li_2O$	503	615	632	824	112	0.53 ± 0.03	0.102 ± 0.004
CaLiBO-30	$67B_2O_3 + 3CaO + 30Li_2O$	492	563	589	876	71	0.23 ± 0.02	0.062 ± 0.004
LiBO	$67B_2O_3 + 33Li_2O$	492	539	561	908	47	0.13 ± 0.01	0.040 ± 0.003

Fig. 1. X-ray diffraction patterns of all glassy samples.

Fig. 2. Differential thermal analysis (DTA) curves for all glass compositions prepared. The characteristic temperatures (T_g, T_{oc}, T_{pc}, T_l) are indicated by arrows.
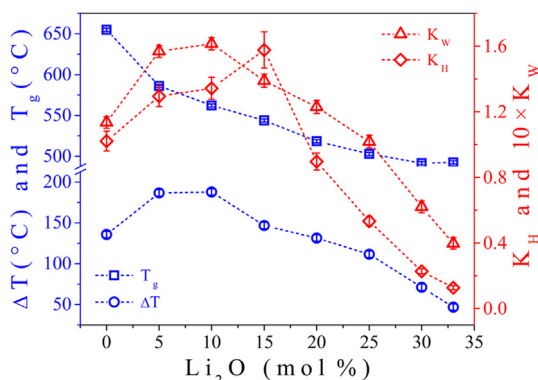
Fig. 3. Glass transition behavior and thermal stability parameters (ΔT, K_H, K_W) as a function of Li_2O content.

sample). It is well known that Li^+ ion provides a lower crosslinking efficiency when compared to Ca^{2+} which exhibits a higher coordination number with oxygen atoms in the glass network [9]. This fact can explain the observed decrease in the T_g. It is possible to consider that the glasses containing up to 25 mol% of Li_2O presents high thermal stability according to ΔT parameter (values higher than 100 °C). The highest thermal stability was obtained to CaLiBO-10 sample, considering ΔT and K_W values, while CaLiBO-15 presented the higher value considering K_H.

3.3. MIR spectra

The absorptions in MIR spectral region of borate glasses are well known and can be observed in three distinct regions. The attributions will consider the symbols Ø = BO (bridging oxygens) and O^- = NBO (non-bridging oxygen). The first region is found between 600 and 800 cm^{-1} being attributed to the bending vibration of borate network consisting of B^3 units. The second region is observed between 800 and 1150 cm^{-1} and is due to B − O stretching vibrations of tetrahedral B^4 SRO units with no presence of NBOs. The third region is observed between 1150 and 1600 cm^{-1} and is due to vibrations of B − Ø and B − O^- bonded to trigonal B^3 and B^2 SRO units, respectively [9–11].

The MIR spectra were obtained on the prepared glasses and the region of interest was selected in the range of 600 to 1600 cm^{-1}, since no significant hydroxyl vibrations were identified. Fig. 4 (A) shows the MIR spectra of the CaBO, CaLiBO-05, and CaLiBO-10 glasses, as well as the Gaussian band decomposition of the MIR spectra of the CaBO glass. Fig. 4 (B) presents the spectra for CaLiBO-10, CaLiBO-20, CaLiBO-30 and LiBO glasses. The spectra obtained for the CaLiBO-15 and CaLiBO-25 samples were omitted from Fig. 4(B) for clarity, because they follow the same trend. As expected, three broad and intense bands were observed and are centered at ~ 693 cm^{-1}, ~ 915 cm^{-1} and ~ 1330 cm^{-1}. The attributions for eight Gaussian peaks related to B − O bond vibrations observed in the spectra were done according to the references [7, 9–11, 19–22] and are summarized in Table 2.

The analysis of MIR spectra in borate glasses is complex due to their broad and extensively overlapping bands. However, it is possible to note that the conversion of trigonal B^2 to B^4 tetrahedral-containing groups are initially favored because of a compositional dependence of the absorption band at 800–1150 cm^{-1} evidenced by the arrows in Fig. 4 (A). This is confirmed by a systematic increase in intensity of the 800–1150 cm^{-1} band for glass compositions containing up to 10 mol% of Li_2O (x < 10) in substitution of CaO. Additionally, the band in the third region (1150 to 1600 cm^{-1}) related to metaborate B^2 units decreases in intensity as further evidence of the conversion of B^2 to B^4 units.

At higher Li_2O contents (x > 10), however, the opposite behavior is observed where B^4 units are converted back to B^2. This result is supported by the systematic decrease in the second band (800 to 1150 cm^{-1}) and the increase in the third band (1150 to 1600 cm^{-1}) as evidenced by the arrows in Fig. 4 (B).

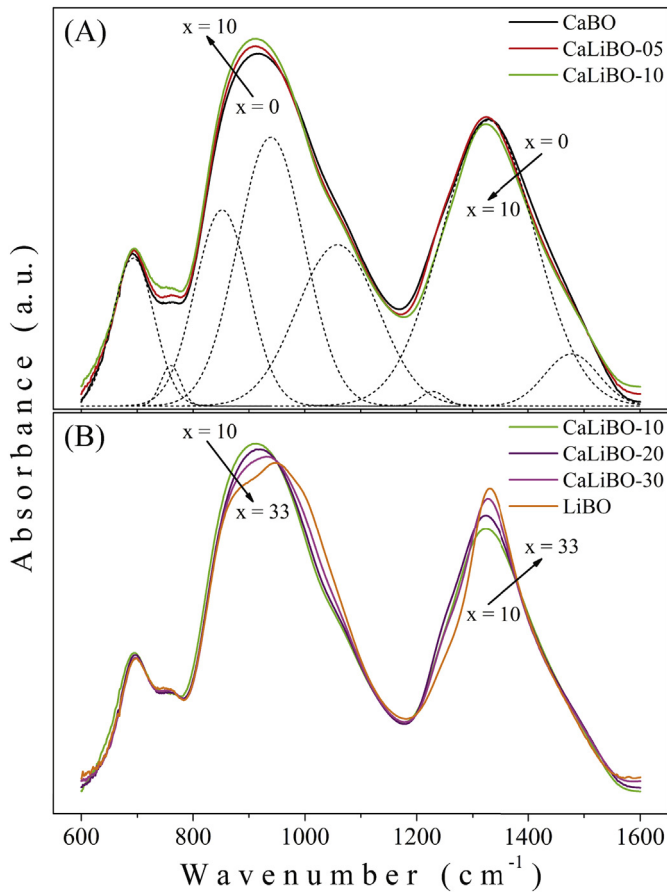In summary, the MIR spectra demonstrate that Li_2O in substitution

Fig. 4. FTIR absorption spectra of (A) CaBO, CaLiBO-05 and CaLiBO-10, and (B) CaLiBO-x (x = 10, 20, 30) and LiBO. Gaussians decomposed bands to the spectra of CaBO sample is shown in (A). Arrows indicates the overall trend of B^4 and B^2 units according to composition (see text).

Table 2
Infrared vibration assignments according to Gaussians decomposed bands.

Peak position (cm^{-1})	Infrared vibration assignments
~ 693	$B - \varnothing - B$ (B^3) bending vibration in borate network
~ 760	Symmetric breathing of six membered rings where one $B\varnothing_3$ (B^3) is replaced by one BO_4^- (B^4) unit
~ 852	$B - \varnothing$ stretching of BO_4^- (B^4) in tri-, tetra- and pentaborate groups
~ 940	$B - \varnothing$ stretching of BO_4^- (B^4) in diborate groups
~ 1059	$B - \varnothing$ stretching of BO_4^- (B^4) in pentaborate groups
~ 1229	$B - \varnothing$ stretching of $[B\varnothing_2O^-]_n$ (B^2) in metaborate chains
~ 1329	$B - O^-$ stretching of $B\varnothing_2O^-$ (B^2) unit in metaborate rings
~ 1478	$B - O^-$ stretching of $[B\varnothing_2O^-]_n$ (B^2) in metaborate chains linked to one BO_4^- (B^4) unit

of CaO in tetraborate glasses is governed by the following isomerization reaction, Eq. (1) [7, 9, 11]:

$$B\varnothing_2O^- \Leftrightarrow B\varnothing_4^- \qquad (1)$$

also designated as $B^2 \Leftrightarrow B^4$ and which determines the SRO and IRO in the glass structure. Li_2O substituting CaO favors the reaction to the right direction, increased B^4 units, due to a progressive transformation of metaborate triangles, B^2, towards borate tetrahedral entities, B^4, for compositions containing up to 10 mol% of Li_2O (x < 10). Glasses with lithium oxide in higher contents (x > 10) favors the reaction to the left, increased B^2 units.
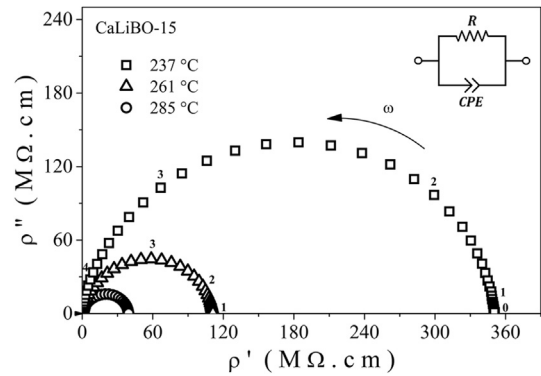

Fig. 5. Impedance spectra, presented in terms of ρ″ versus ρ′ complex plane plots, measured on the CaLiBO-15 in three different temperatures. Numbers indicate the logarithm of signal frequency. Fitting data considered a modified-Debye model involving the use of a constant-phase element (see text), the Debye R-C circuit model being the one shown in the inset.

3.4. Impedance spectroscopy

Fig. 5 shows a representative IS spectra (in terms of complex resistivity, ρ^*) of CaLiBO-15 sample for three different temperatures. The IS spectra of all samples showed the same semicircular trend and were fitted considering the glass bulk material as an equivalent circuit formed by a resistor, R, in parallel to a Constant-Phase Element (CPE). For this combination, the impedance can be represented by Eq. (2):

$$Z^*_{R||CPE}(\omega) = \frac{R}{1 + (i\omega\tau_0)^\alpha} \qquad (2)$$

where ω is the angular frequency, τ_0 is the relaxation time and α ($0 \leq \alpha \leq 1$) is related to a decentralization angle expressed in radian by $\theta = (1 - \alpha)\frac{\pi}{2}$ [23]. Values of decentralization angle are related with a distribution of relaxation times and can be associated with an intrinsic structural disorder of the material, where lower values of α (higher decentralization) corresponds to a more disordered structure. Fig. 6 shows the behavior of the α factor obtained from the fitting of the IS spectra for all glass compositions in different temperatures. It is seen that α values decrease with the addition of Li_2O which reflects the lower crosslinking of Li^+ ions [9]. Further, the values of the α factor tend to increase to unity as the temperature decreases, and eventually, at lowest temperatures, were set as a unity in order to satisfy the theoretical condition, $\alpha \leq 1$. It was observed, not shown, that the dielectric permittivity, ε_∞, increases with temperature and with the concentration of Li^+ ions (x). Values of capacitance found for all samples studied in this work stay in the order of 10^{-12} to 10^{-11} F, which is further evidence that the observed impedance semicircle is related to the volume (bulk) conduction process [24, 25].
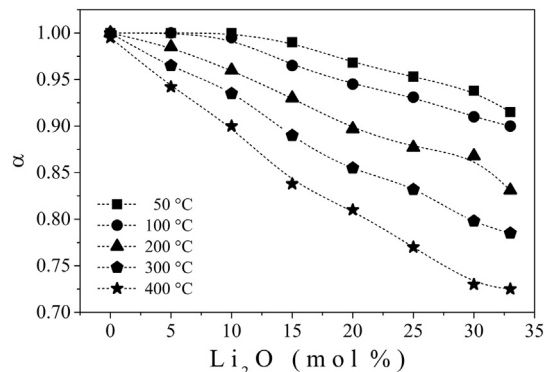

Fig. 6. Decentralization angle factor α as a function of Li_2O content for different temperatures.
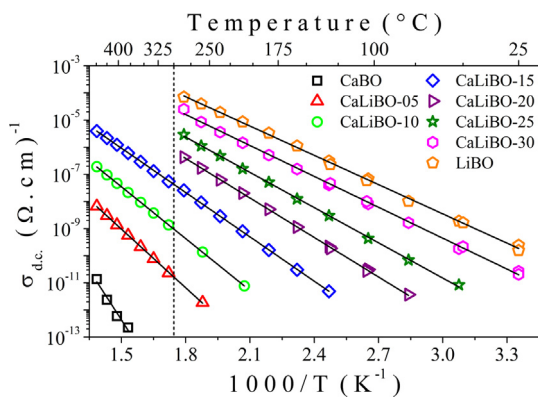
Fig. 7. Arrhenius plot for d.c. electrical conductivity values of all vitreous samples. The dashed line is a guide for the eyes to facilitate comparison of conductivity values at 300 °C (see text).
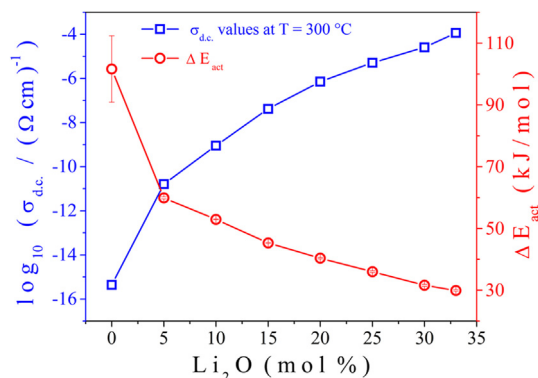

Fig. 8. Activation energy (ΔE_{act}) and log values of ionic conductivity ($\sigma_{d.c.}$) at 300 °C as a function of Li_2O content.

All adjustments were achieved in terms of the impedance relation described above and by considering $\rho^* = (A/t)Z^* = (A/t)$ $(Z' - iZ'') = \rho' - i\rho''$, where (A/t) corresponds to the ratio of the area and thickness of each sample. The d.c. ionic conductivity, $\sigma_{d.c.} = 1/\rho^*(\omega \to 0)$, can be found considering the resistivity values obtained from the glass bulk semicircle diameter in the Nyquist plot, as shown in Fig. 5. It is worth to mention that the electrode polarization contribution starts to be present in the impedance spectra for compositions with $x > 20$. This effect can be taken into account adding and extra parallel-CPE in the equivalent circuit model. This addition provides a better achievement of the fitting process resulting in more accurate values for the bulk ionic conductivity. Values of the $\sigma_{d.c.}$ are shown in Fig. 7, as a function of inverse of the absolute temperature. It is seen that the addition of lithium in the structural composition of CaB_4O_7 ($x = 0$) considerably increases its conductivity up to $Li_2B_4O_7$ ($x = 33$) composition. The increase in conductivity may be initially attributed to the favoring conversion of boron trigonal to boron tetragonal units ($0 < x \leq 10$). Each B^4 tetrahedron has a negative (delocalized) charge and the alkali cations are located in the vicinity of these negative sites, making ion transport possible. Nonetheless, when Li^+ ions are present ($x \geq 5$) the ionic conductivity continuously increases and it is mainly associated to an increase of Li^+ charge carriers and its higher mobility, which can be attributed to the chemical bonding energy in a four-fold coordination and also to the effective size of the ion (ionic radius = 0.59 Å), which is known to be smaller than the divalently charged Ca^{2+} ion (ionic radius = 1.00 Å) with a six-fold coordination [26].

In order to emphasize the increase of the ionic conductivity, Fig. 8 shows the behavior of the ionic conductivity as a function of glass compositions at 300 °C. These values were estimated from the linear fit parameters of Fig. 7, considering an Arrhenius behavior, described by

Eq. (3) [26]:

$$\sigma(T) = \frac{\sigma_0}{T} \, exp\left(-\frac{\Delta E_{act}}{k_B T}\right) \tag{3}$$

It is impressive to note that the ionic conductivity increases 10 orders of magnitude (10^{-15} S/cm for CaBO to 10^{-4} S/cm for LiBO, at 300 °C) with the substitution of calcium by lithium.

From Eq. (3) it is possible to access the activation energy (ΔE_{act}) which is related to the energy barrier for the conductivity process that depends on the ions mobility into the glass. Calculated activation energy values for the conductivity processes of the glass matrix are also shown in Fig. 8. It can be observed that the exchange of calcium by lithium significantly reduces the activation energy of the conduction process. This behavior is close related with the lower crosslinking efficiency provided by Li^+ ions, in a similar trend as T_g temperatures shown in Fig. 3.

4. Conclusions

Tetraborate glasses with a gradual substitution of CaO by Li_2O in the $xLi_2O + (33-x)CaO + 67B_2O_3$ system were prepared by the conventional melting and casting method. The obtained samples were homogeneous, bubble free, transparent and presented no crystallization as confirmed by X-ray diffractometry (XRD).

Characteristic temperatures and thermal stability parameters were obtained by DTA analysis. The results demonstrate a decrease in the glass transition temperature as calcium is replaced by lithium ions. Thermal stability evaluated by ΔT, K_H and K_W parameters had shown high values for glasses with Li_2O content up to 20 mol% (CaLiBO-20). The highest thermal stability was observed to CaLiBO-10 sample, considering ΔT and K_W values being (188 ± 4) °C and (0.161 ± 0.004) °C, respectively.

The short and intermediate order of the glass structures has demonstrated to be governed by the $B\emptyset_2O^- \Leftrightarrow B\emptyset_4^-$ ($B^2 \Leftrightarrow B^4$) isomerization reaction. Lithium ions in substitution of calcium favors the transformation of metaborate triangles, B^2 units, in borate tetrahedral entities, B^4 units, for compositions up to 10 mol% of Li_2O ($x < 10$) by following the right direction of the reaction. This structural arrangement may lead to the increase in glass thermal stability parameters, as seen in DTA results. Glasses containing lithium oxide in higher contents ($x > 10$) will promote the reaction occurring in the opposite direction.

IS results shows an increase of the electrical conductivity with the increase of the Li^+ ion concentration up to the LiBO composition ($x = 33$), reaching variations greater than 10 orders of magnitude, when evaluated at 300 °C. The decentralization of the impedance arcs, represented by the α factor, and the diminish in activation energy values also indicate that the addition of lithium tends to increase the heterogeneity of the glass network. The glass transition temperature, as well as electrical conductivity and activation energy values shows a strong dependence on the type of the metallic modifier ion (M), and the strength of the M − O interaction in this case of mixed modifier tetraborate glasses.

References

[1] J. Zhong, P.J. Bray, Change in boron coordination in alkali borate glasses, and mixed alkali effects, as elucidated by NMR, J. Non-Cryst. Solids 111 (1989) 67–76.

[2] W.J. Clarida, et al., Dependence of N_4 upon alkali modifier in binary borate glasses, Phys. Chem. Glasses 44 (3) (2003) 215–217.

[3] A.C. Wright, N.M. Vedishcheva, Superstructural unit species in vitreous and crystalline alkali, alkaline earth and related borates, Phys. Chem. Glasses Eur. J. Glass Sci. Technol. B 54 (4) (2013) 147–156.

[4] Y. Xue, J. Cao, Z. Zhang, L. Wang, S. Xu, M. Peng, Manipulating Bi NIR emission by adjusting optical basicity, boron and aluminum coordination in borate laser glasses, J. Am. Ceram. Soc. 101 (2018) 624–633.

[5] N. Sdiri, H. Elhouichet, M. Ferid, Effects of substituting P_2O_5 for B_2O_3 on the thermal and optical properties of sodium borophosphate glasses doped with Er, J. Non-Cryst. Solids 389 (2014) 38–45.

[6] V.A. Silva, M.L.F. Nascimento, P.C. Morais, N.O. Dantas, The structural role of Ti in a thermally-treated $Li_2O-B_2O_3-Al_2O_3$ glass system, J. Non-Cryst. Solids 404 (2014) 104–108.

[7] S.S. Rojas, J.E. De Souza, K. Yukimitu, A.C. Hernandes, Structural, thermal and optical properties of CaBO and CaLiBO glasses doped with Eu^{3+}, J. Non-Cryst. Solids 398-399 (2014) 57–61.

[8] B. Padlyak, W. Ryba-Romanowski, R. Lisiecki, O. Smyrnov, A. Drzewiecki, Burak Ya, V. Adamiv, I. Teslyuk, Synthesis and spectroscopy of tetraborate glasses doped with copper, J. Non-Cryst. Solids 356 (2010) 2033–2037.

[9] Y.D. Yiannopoulos, G.D. Chryssikos, E.I. Kamitsos, Structure and properties of alkaline earth borate glasses, Phys. Chem. Glasses 42 (3) (2001) 164–172.

[10] E.I. Kamitsos, A.P. Patsis, M.A. Karakassides, G.D. Chryssikos, Infrared reflectance spectra of lithium borate glasses, J. Non-Cryst. Solids 320126 (1990) 52–67.

[11] E.I. Kamitsos, G.D. Chryssicos, Borate glass structure by Raman and infrared spectroscopies, J. Mol. Struct. 247 (1991) 1–16.

[12] S.W. Martin, C.A. Angel, Glass formation and transition temperatures in sodium and lithium borate and aluminoborate melts up to 72 mol.% alkali, J. Non-Cryst. Solids 66 (1984) 429–442.

[13] N.P. Lower, J.L. McRae, H.A. Feller, A.R. Betzen, S. Kapoor, M. Affatigato, S.A. Feller, Physical properties of alkaline-earth and alkali borate glasses prepared over an extended range of compositions, J. Non-Cryst. Solids 293-295 (2001) 669–675.

[14] I.I. Kindrat, B.V. Padlyak, R. Lisiecki, Judd–Ofelt analysis and radiative properties of the Sm^{3+} centres in $Li_2B_4O_7$, CaB_4O_7, and $LiCaBO_3$ glasses, Opt. Mater. 49 (2015) 241–248.

[15] E.B. Ferreira, E.D. Zanotto, S. Feller, G. Lodden, J. Banerjee, T. Edwards, M. Affatigato, Critical analysis of glass stability parameters and application to lithium borate glasses, J. Am. Ceram. Soc. 1 (9) (2011).

[16] S.I. Amma, M.T. Lanagan, S.H. Kim, C.G. Pantano, Ionic conductivity in sodium-alkaline earth-aluminosilicate glasses, J. Am. Ceram. Soc. 99 (4) (2016) 1239–1247.

[17] M.L.F. Nascimento, L.A. Souza, E.B. Ferreira, E.D. Zanotto, Can glass stability parameters infer glass forming ability? J. Non-Cryst. Solids 351 (40–42) (2005) 3296–3308.

[18] I. Avramov, E.D. Zanotto, M.O. Prado, Glass-forming ability versus stability of silicate glasses. II. Theoretical demonstration, J. Non-Cryst. Solids 320 (2003) 9–20.

[19] S.S. Rojas, K. Yukimitu, A.S.S. Camargo, L.A.O. Nunes, A.C. Hernandes, Undoped and calcium doped borate glass system for thermoluminescent dosimeter, J. Non-Cryst. Solids 352 (2006) 3608–3612.

[20] I. Ardelean, B. Pascuta, Comparative vibrational study of xFe_2O_3-(1 x)$[3B_2O_3$-MO] (MO = CaO or CaF_2) glass systems, Mater. Lett. 58 (2004) 3499–3502.

[21] E. Mansour, Structure and electrical conductivity of new $Li_2O–CeO_2–B_2O_3$ glasses, J. Non-Cryst. Solids 357 (2011) 1364–1369.

[22] G.D. Chryssikos, J.A. Kapoutsis, E.I. Kamitsos, A.P. Patsis, A.J. Pappin, Lithium-sodium metaborate glasses: structural aspects and vitrification chemistry, J. Non-Cryst. Solids 167 (1994) 92–105.

[23] J.R. Macdonald, Impedance Spectroscopy - *emphasizing solid materials and systems*, John Willey & Sons, New York, 1987 346 p. (0471831220).

[24] J.T.S. Irvine, D.C. Sinclair, A.R. West, Electroceramics: characterization by impedance spectroscopy, Adv. Mater. 2 (3) (1990) 132–138.

[25] M.F. García-Sánchez, J.-C. M'Peko, A.R. Ruiz-Salvador, G. Rodríguez-Gattorno, Y. Echevarría, F. Fernández-Gutierrez, A. Delgado, An elementary picture of dielectric spectroscopy in solids: physical basis, J. Chem. Educ. 80 (9) (2003) 1062–1073.

[26] S.W. Martin, Glass and Glass-Ceramic Sulfide and Oxy-Sulfide Solid Electrolytes. Handbook of Solid State Batteries: 2nd, (2015), pp. 433–450.